SAND2017-7188C

Characterization of Electrochemical Surface Area and Porosity of Zirconia Sensors

Lok-kun Tsui,[a] Angelica Benavidez,[a] Lindsey Evans,[b] Fernando Garzon[a,b]

[a] Center for Micro-Engineered Materials, University of New Mexico, Albuquerque, NM, 87106

[b] Advanced Materials Laboratory, Sandia National Laboratories, Albuquerque, NM, 87106

Solid-state zirconia sensors are used in a wide variety of applications including controlling the air to fuel ratio in combustion engines and pollution monitoring. These sensors use either a layer of zirconia as a solid-state ionic electrolyte or a gas-porous ceramic as a protective layer. There is a need for quantitative methods to assess the tortuosity of these porous layers and the size of the electrode area exposed which can be performed on completed sensor devices. We demonstrate using electrochemical double layer capacitance and transport studies in aqueous potassium ferri/ferro-cyanide electrolytes that these parameters can be readily measured. The technique is demonstrated on sensors procured from ESL ElectroScience as well as sensors produced in-house using additive manufacturing. The processes that we develop can be applied as quality control to ensure sample-to-sample reproducibility of the porous layer.

Introduction

Zirconia based sensors are used in a large number of gas detection applications.[1–3] A component common to many zirconia sensors is a porous layer that serves as either an inert protective layer, a diffusion limiting layer, or an electrolyte.[4–6] Figure 1 shows simplified schematics of (a) a lambda oxygen sensor, (b) an amperometric diffusion limiting current sensor, and (c) a mixed potential sensor. Lambda oxygen sensors in automobiles use the difference in the Nernst potential for oxygen between an electrode exposed to exhaust gas and an air reference to sense the concentration of oxygen in the exhaust.[2] Wide-band oxygen sensors use an amperometric pumping cell where exhaust gas is directed through a pinhole opening and passed through a diffusion barrier to an electrode where oxygen is pumped through the YSZ electrolyte. The diffusion limiting current is used to sample a broader range of oxygen concentrations compared to the Lambda oxygen sensors.[7,8] The output from either type of oxygen sensor can be used by the vehicle's on-board computer to regulate the mixture of air and fuel for optimal performance and minimize emissions. Mixed potential sensors can be used as gas analyzers for emissions control or pollution monitoring. The gases of interest in a mixed potential sensor diffuse through the porous yttria stabilized zirconia (YSZ) layer and the mixed potential established by the difference in the electrochemical kinetics at three-phase interface of each electrode serves as a sensing parameter.[9,10]

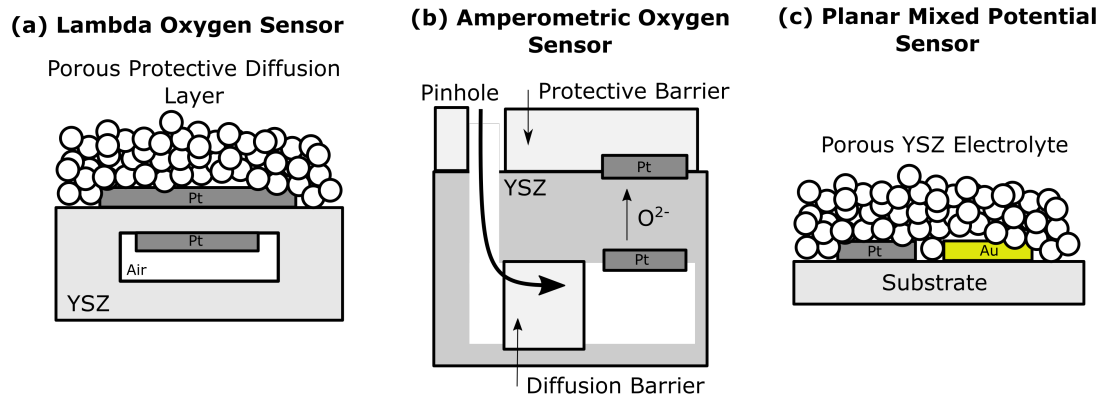

Figure 1. Schematics of (a) a Lambda oxygen sensor with a porous protective barrier, (b) an amperometric oxygen sensor with both a porous diffusion barrier and a protective barrier, and (c) a Pt/Au mixed potential sensor with a porous YSZ electrolyte. Gases must diffuse through porous layers in all three devices.

We are pursuing a project where mixed-potential sensors can be additively manufactured for rapid prototyping, and quality control techniques are required to ensure the reproducibility of the printed porous layers. Materials parameters of interest include the exposed Pt surface area beneath the porous YSZ electrolyte and the tortuosity through the porous layer to the electrodes. Gas phase adsorption and desorption measurements can be useful in studying the porosity of materials in powder form,[11,12] but are often times unsuitable for characterizing transport properties of porous layers deposited onto sensor substrates due to low sample surface areas. The use of electrochemical impedance of the electrode has also been investigated for characterizing the diffusion and tortuosity through porous electrodes. For example, Fu et al. developed diffusional models to relate the impedance response as a function of gas pressure to the tortuosity of solid oxide fuel cell electrodes.[13] Finally, the limiting current of oxygen reduction can be correlated to the diffusivity of gases through the porous layer.[14] For the mixed potential sensors of the configuration investigated here, the partial pressure of oxygen must be brought below extremely low concentrations for the limiting current to be detected. Measuring the diffusion coefficients in aqueous electrolytes is more practical because the diffusion of ions in liquids are orders of magnitude slower than in the gas phase, and can more easily differentiate between samples with varying porosity and tortuosity.

We report on the application of simple aqueous electrochemical techniques to assess the surface area of the underlying platinum electrodes and the diffusion of ions through the porous layer to the electrodes in both commercially produced sensors and sensors prepared by additive manufacturing. Double layer capacitance measurements are used to measure the exposed surface area, and the maximum current of the oxidation and reduction of $Fe(CN)_6^{-3,-4}$ ions during cyclic voltammetry are used to measure the effective diffusion coefficient through the porous layer. This redox reaction is chosen because the oxidation and reduction of $Fe(CN)_6^{-3,-4}$ is a simple outer-shell electron transfer reaction which has no kinetic barriers associated with chemical bond fragmentation or formation.[15] We demonstrate that we detect differences in the diffusion coefficient among commercially prepared samples and a difference in the exposed surface area between commercially

prepared and additively manufactured sensors. These techniques are simple to carry out and should prove useful as a quality control technique to ensure that the porous layer is consistently manufactured.

Experimental Section

Sensor Fabrication

Five mixed-potential sensors (Figure 2) were obtained from ESL ElectroScience consisting of a 3-electrode $La_{0.8}Sr_{0.2}CrO_3$ (LSCO), $Au_{0.5}Pd_{0.5}$, and Pt device, three LSCO+Pt sensors with varying geometries, and an LSCO+Pt device with a highly porous alumina overcoat 100 μm thick. ESL sensors are produced by screen printing each of these components onto laminated YSZ green tape and co-firing.

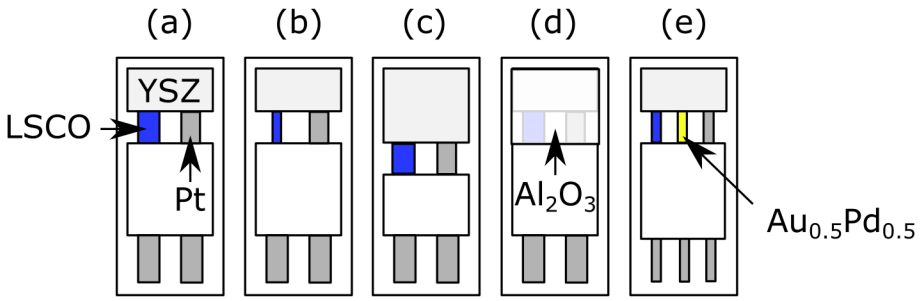

Figure 2. Schematic representation of mixed potential sensors obtained from ESL ElectroScience. (a) LSCO|YSZ|Pt sensor with wide LSCO electrode, (b) LSCO|YSZ|Pt sensor with thin LSCO electrode, (c) LSCO|YSZ|Pt sensor with double size YSZ electrolyte, (d) LSCO|YSZ|Pt sensor with alumina coating, (e) Three electrode LSCO+Au/Pd+Pt sensor.

Sensors were manufactured using a controlled micro-extrusion method. The Pt electrode was printed on YSZ green tape (ESL 42000) using a Pt ink (ESL 5570) and these two materials were co-fired at 1450°C. The second electrode was printed using a paste consisting of $La_{0.87}Sr_{0.13}CrO_3$ powder (Praxair) and ESL vehicle and thinner (ESL 473 and ESL 401, respectively). The device was fired at 1200°C. The YSZ electrolyte was printed using a paste consisting of YSZ powder (Tosoh, TZ-3YS) and the previously mentioned vehicle and thinner and then fired at 1100°C. Two sensors were manufactured using inks and pastes that were extruded by hand while one sensor was made with components extruded from a mechanical printer controlled by CAD software.

The morphology of the Pt electrodes of the printed sensors and ESL's sensors were examined by scanning electron microscopy. The thicknesses of the YSZ layer on all sensor samples were measured using stylus profilometry with a Bruker DektatXT system.

Measurement of Pt Surface area and Effective Diffusion Constant

All electrochemical measurements were performed in a 3-electrode cell (Pine Research Instrumentation, AKCELL1) with an Ag/AgCl (sat. KCl) reference electrode, and a Pt coil counter electrode (Pine Research Instrumentation, AFCTR5). The tests on sensors were compared to a 3.0 mm diameter Pt disk electrode (Pine Research Instrumentation,

AFE1XFG030PTR). A PAR 2273 potentiostat (Princeton Applied Research) was used for all electrochemical measurements. Prior to electrochemical testing on the sensors, a Cu wire was connected to the Pt lead on each sensor by Ag-Sn soldering or Ag epoxy. The connection was reinforced by J-B Weld epoxy and the area of the YSZ electrolyte above the Pt electrode was isolated by applying a minimum of 4 coats of acrylic nail polish to insulate the rest of the sensor.

The surface area of the exposed underlying Pt electrodes was determined using double layer capacitance in a solution of 0.1M H_2SO_4. First, 10 cycles of cyclic voltammetry (CV) were obtained in a window from -0.3 to 1.0 V vs. Ag/AgCl at a scan rate of 200 mV/s to clean the surface. In some cases the hydrogen adsorption/desorption region of the Pt CV could be observed, however the low surface areas precluded accurate integration of the hydrogen surface charge. Next, 30 cycles were taken between 0.5 and 0.7 V vs. Ag/AgCl at scan rates varying between 300 and 50 mV/s. Since capacitance is the proportionality constant between current and scan rate (Equation 1), the slope of the current density vs scan rate curve is used to obtain the double layer capacitance.

$$Q = CV; \frac{dQ}{dt} = I = C\frac{dV}{dt} \quad [1]$$

The current is first normalized to the geometric area of the electrode, and the double layer capacitance is then used to calculate the roughness factor with a normalization constant of 20 μF/cm^2 for Pt.[16]

The effective diffusion coefficient measurements were performed in 0.1M $K_3Fe(CN)_6$, 0.1M $K_4Fe(CN)_6$, and 0.05M Na_2SO_4 by taking 30 CVs scanning between -0.25 to 0.75 V vs. Ag/AgCl. The high ionic conductivity of the solution minimizes the ionic transport due to electrostatic migration. Scan rates were varied between 300 and 50 mV/s. We assume that the diffusion coefficient in solution is much greater than the diffusion coefficient through the porous layer so that the one through the porous layer is the dominant term. The peak current density of the reduction and oxidation of $Fe(CN)_6^{-3,-4}$ were fitted to the Randles-Sevcik equation[17] (Equation 2) using the Python numerical package SciPy (Version 0.16.0). In the Randles-Sevcik equation j_p is the magnitude of the peak current density, n is the number of electrons transferred in the redox reaction, C is the concentration in the bulk, and ν is the scan rate. The current density is normalized to the real surface of the exposed Pt beneath the porous layer using the value obtained through double layer capacitance measurements.

$$j_p = 2.68\,x10^5\, n^{\frac{3}{2}} D^{\frac{1}{2}} C v^{\frac{1}{2}} \quad [2]$$

Results and Discussion

Exposed surface area of Pt electrodes

Figure 3 shows the cyclic voltammetry of the Pt electrode on the ESL 3-electrode sensor in 0.1M H_2SO_4 with scan rates varied from 50 to 300 mV/s. As expected of current associated with the charging of the double layer, the width of the CV increases linearly with increasing scan rate. The current density normalized to the geometric area of the Pt electrodes at 0.6 V vs. Ag/AgCl was used to as the capacitive current and is fit with a line to obtain the double layer capacitance. The results of the surface area measurements on the

sensors and a Pt disk are shown in Table I. The roughness factor of the sensor samples varies from a minimum of 1.6 to a maximum of 5.4.

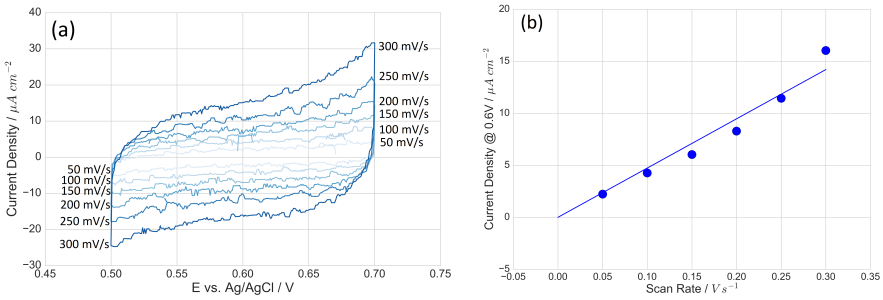

Figure 3. (a) Cyclic voltammetry of the Pt electrode of the ESL 3-electrode sensor and (b) a linear fit of the current density at the center of the sweep window used to obtain capacitance.

TABLE I. Double layer capacitance and associated roughness factor of a reference Pt disk and several commercial mixed potential sensors.

Sample Name	DL Capacitance (μF/cm^2)	Roughness Factor
Pt Disk	24.2	1.2
Wide LSCO Sensor	50.0	2.5
Thin LSCO Sensor	89.7	4.5
3 Electrode Sensor	47.4	2.4
Alumina Coated	31.3	1.6
Double Size	107.1	5.4

Effective Diffusion Constants Through the Porous Layer

Figure 4(a) shows the cyclic voltammetry of the Pt electrode from the 3-electrode sensor for oxidation and reduction of ferri/ferro-cyanide. The peaks are symmetric for oxidation and reduction, centered about the redox potential of 250 mV vs. Ag/AgCl, and increase in magnitude with increasing sweep rate. Figure 4(b) shows the fit of the peak current density to the Randles-Sevcik equation which is done separately for oxidation and reduction reactions. CVs and fits to the Randles-Sevcik equation were obtained for all the sensors. All data has been normalized to the real surface area obtained by double layer capacitance. The effective diffusion constants are shown in Table II. The Pt disk without any porous layer exhibits an effective diffusion constant on the order of 10^{-6} cm^2/s, which is consistent with the values reported by Konopka and McDuffie for thinly separated Pt plates.[18] The diffusion constants on the sensors are all less than that of a Pt disk, indicating that the presence of the porous layer inhibits ionic diffusion to the Pt electrode. The effective diffusivity among the different samples varies across three orders of magnitude from a minimum of 10^{-10} cm^2/s to a maximum of 10^{-7} cm^2/s. The alumina coated sample is among the ones with the highest diffusion constant, so the presence of this physical protection layer does not inhibit the transport as much as the underlying porous YSZ layer does. To rule out that this effect is a result of simple differences in thickness, profilometry (Table II, 4th column) reveals that the thickness of the YSZ layers on these sensors is not correlated with the diffusion coefficient measured. The differences must therefore result from variations in porosity intrinsic to the YSZ layer. These results demonstrate that we can

detect differences in the diffusion of ions through porous layers from batch to batch of samples, a parameter which we find is not well controlled in these commercial samples.

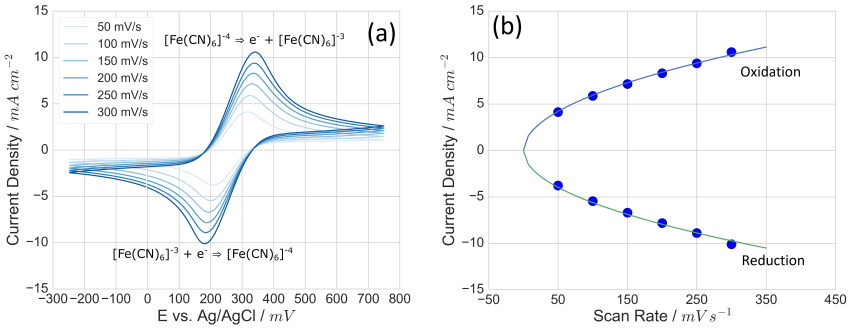

Figure 4. (a) Cyclic voltammetry of the three-electrode sensor in Ferri/ferro-cyanide solutions showing symmetric peaks associated with oxidation and reduction at different scan rates. For each scanrate, the 30th cycle is shown. (b) Fit of the peak of the oxidation and reduction peaks (dots) to the Randles-Sevcik equation (solid lines).

TABLE II. Effective diffusion constant of Pt electrodes in disk form, and as electrodes beneath porous YSZ layers. Pt plates data from ref. 13.

Sample Name	D_{Eff} – Oxidation (cm^2/s)	D_{Eff} – Reduction (cm^2/s)	YSZ Thickness (μm)
Pt Plates[18]	7.26×10^{-6}	6.67×10^{-6}	N/A
Pt Disk	4.61×10^{-6}	3.84×10^{-6}	N/A
Wide LSCO Sensor	7.06×10^{-10}	6.54×10^{-10}	64
Thin LSCO Sensor	3.52×10^{-8}	3.24×10^{-8}	70
Three Electrode Sensor	4.90×10^{-7}	4.35×10^{-7}	98
Alumina Coat	3.47×10^{-7}	3.13×10^{-7}	64
Double Size	6.15×10^{-8}	5.51×10^{-8}	64

Characterization of Additively Manufactured Sensor Prototypes

The application of these techniques to additively manufactured sensors represents an opportunity to implement quality control procedures in the fabrication process. We have tested three prototypes in this set of experiments: two hand-printed sensors and one prepared by machine extrusion from a computer controlled printer. Figure 5(a) shows a plot of the capacitive current as a function of scan rate, comparing the three prototypes with the capacitive current from the 3-electrode sensor from ESL. The roughness factors are 20-80x larger in the additively manufactured prototypes than the average of the roughness factors reported of the commercially produced devices in Table I. Scanning electron microscopy comparing the Pt electrodes from ESL's 3-electrode sensor and the additively manufactured sensors shows that Pt produced by additive manufacturing in Figure 5(b) achieved a final particle size in the range of 200-400 nm with visible porosity, while the Pt on the ESL 3-electrode sensor in Figure 5(c) consists of densely packed 1-5 μm sized particles. Quantitative surface area measurements and the effective diffusion

coefficients are listed in Table III. After normalization to the true Pt surface area, the diffusion constants are between 10^{-10} and 10^{-8} cm^2/s, within the range exhibited by the sensors obtained from ESL. The highest diffusion coefficient is obtained from the machine printed sample, where fine control of the deposition by the printer allows us to produce a thinner layer compared to the hand extruded samples. Profilometry indicates a range of thickness from 66 μm up to 140 μm, and the diffusion coefficient is negatively correlated with sample thickness. These results indicate that the YSZ layer produced by additive manufacturing has similar inhibitive effects to the transport of $Fe(CN)_6^{-3,-4}$ as the YSZ layer on commercially obtained sensors, and thicker layers inhibit the transport more strongly.

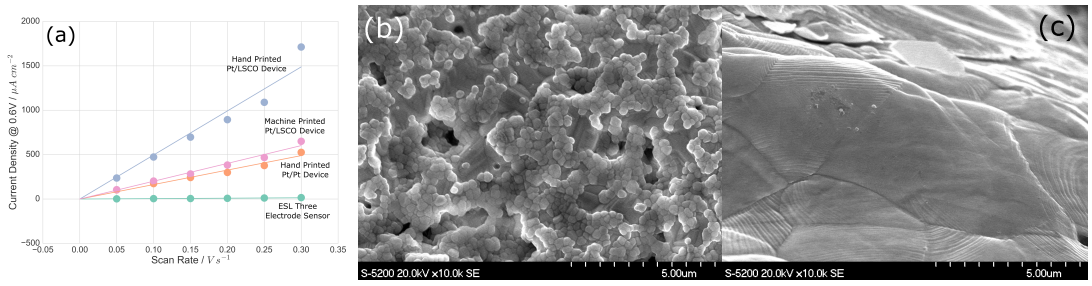

Figure 5. (a) Current density as a function of scan rate, comparing three additively manufactured sensor prototypes with the 3-electrode sensor from ESL. Scanning electron microscopy shows that the surface area of (b) the additively manufactured samples has a smaller particle size and visible porosity compared with (c) densely sintered Pt on the ESL 3-electrode sensor.

TABLE III. Surface area measurements and effective diffusion constant for additively manufactured sensor prototypes.

Sample Name	Roughness Factor	D_{Eff} - Oxidation (cm^2/s)	D_{Eff}- Reduction (cm^2/s)	YSZ Thickness (μm)
Hand Printed Pt/YSZ/Pt	81.5	2.70×10^{-9}	2.43×10^{-9}	104
Hand Printed Pt/YSZ/LSCO	248	3.51×10^{-10}	2.98×10^{-10}	140
Machine Printed Pt/YSZ/LSCO	100	1.39×10^{-8}	1.26×10^{-8}	66

Conclusions

We have demonstrated the capability to easily characterize the porous YSZ layers of mixed potential sensors sourced from a commercial supplier and our additively manufactured prototypes. The Pt surface area of additively manufactured sensors was found to be 20-100 times higher than the ones on the ESL sensors because of a smaller Pt particle size. The effective diffusion coefficient was determined by cyclic voltammetry and the transport through additively manufactured YSZ layer was comparable to that of the commercial sensors. We find the thickness of the printed layers of our prototypes to be negatively correlated with the diffusion constant. We anticipate that this technique will be an effective

means of characterizing the porous layer of zirconia sensors to ensure that they are reproducibly manufactured.

Acknowledgements

We acknowledge funding from the University of New Mexico, Center for Micro-Engineered Materials.

References

1. E. Ivers-Tiffée, K. H. Härdtl, W. Menesklou, and J. Riegel, *Electrochim. Acta*, **47**, 807–814 (2001).

2. R. Moos, *Int. J. Appl. Ceram. Technol.*, **413**, 401–413 (2005).

3. N. Miura, T. Sato, S. A. Anggraini, H. Ikeda, and S. Zhuiykov, *Ionics.*, **20**, 901–925 (2014).

4. E. L. Brosha, R. Mukundan, D. R. Brown, F. H. Garzon, and J. H. Visser, *Solid State Ionics*, **148**, 61–69 (2002).

5. P. K. Sekhar et al., *Sensors Actuators, B Chem.*, **144**, 112–119 (2010).

6. R. Mukundan, E. L. Brosha, and F. H. Garzon, *J. Electrochem. Soc.*, **150**, H279 (2003).

7. R. Ramamoorthy, P. K. Dutta, and S. A. Akbar, **8**, 4271–4282 (2003).

8. N. Docquier and S. Candel, *Prog. Energy Combust. Sci.*, **28**, 107–150 (2002).

9. J. W. Fergus, *J. Solid State Electrochem.*, **15**, 971–984 (2011).

10. F. H. Garzon, R. Mukundan, and E. L. Brosha, *Solid State Ionics*, **136–137**, 633–638 (2000).

11. M. B. Sweatman and N. Quirke, *Langmuir*, **17**, 5011–5020 (2001).

12. Q. Huang, M. Eić, H. Xiao, and S. Kaliaguine, *Adsorption*, **16**, 531–539 (2010).

13. Y. Fu et al., *J. Electrochem. Soc.*, **162**, F613–F621 (2015).

14. R. E. Williford, L. a. Chick, G. D. Maupin, S. P. Simner, and J. W. Stevenson, *J. Electrochem. Soc.*, **150**, A1067 (2003).

15. A. J. Bard and L. R. Faulkner, *Electrochemical Methods: Fundamentals and Applications*, 2nd ed., p. 471, John Wiley & Sons, New York, NY, (2001).

16. T. Pajkossy and D. M. Kolb, *Electrochim. Acta*, **46**, 3063–3071 (2001).

17. C. H. Hamann, A. Hamnett, and W. Vielstich, in *Electrochemistry*,, p. 236–247, Wiley-VCH, Weinheim, Germany (1998).

18. S. J. Konopka and B. McDuffie, *Anal. Chem.*, **42**, 1741–1746 (1970).